Multi-modal nonlinear dynamic response of cable-stayed beams with two-to-one internal resonance: Theory and experiments

Multi-modal dynamics in cable-stayed beams with two-to-one internal resonance: Theory and experiments

Jian Peng[a,*], Yanan Li[a], Lianhua Wang[b,*], Xiaoyu Zhang[c] and Stefano Lenci[d]

[a]School of Civil Engineering & Hunan Provincial Key Laboratory of Structures for Wind Resistance and Vibration Control, Hunan University of Science and Technology, Xiangtan, Hunan 411201, PR China
[b]College of Civil Engineering Hunan University,Changsha,Hunan 410082,China
[c]Guangxi Communications Design Group Co, Ltd, Nanning 530022, China
[d]Department of Civil and Building Engineering and Architecture, Polytechnic University of Marche, Ancona 60131, Italy

ARTICLE INFO

Keywords:
cable-stayed beam
two-to-one internal resonance
multi-modal dynamics
nonlinear response
interactions

ABSTRACT

In this study, the large-amplitude vibrations and nonlinear modal interactions of a cable-stayed beam under principal resonance excitation with theories and experiments are investigated, focusing on the 2:1 internal resonance between different modes. An accurate description of the interaction in the cable-stayed beam is obtained using the Hamilton variational principle, which leads to the derivation of the equations of motion for the system. A multi-modal discrete model of the cable-stayed beam is subsequently developed through a functional form approach. The method of multiple scales is employed to derive the averaged equations and second-order approximate displacement expressions. The equilibrium and dynamic responses of the cable-stayed beam under various principal resonance conditions are subsequently analyzed. The chaotic dynamics in the unstable region are also analyzed based on numerical simulations and experimental studies. It is found that the nonlinear response of the cable-stayed beam undergoes various bifurcations, displaying a rich spectrum of nonlinear dynamics. Finally, the effects of the interactions between cable and beam, the nonlinearity of beam are discussed.

1. Introduction

Cable-stayed beams, consisting of intricately connected cables and beams, form the backbone of cable-stayed bridges, playing a crucial role in their structural integrity. The interaction between these components is essential for understanding the complex vibrational behavior of the bridge. The dynamic response of cable-stayed bridges is heavily influenced by the behavior of the cable-stayed beams, particularly under varying environmental conditions and load scenarios. However, the complex vibrational behavior and resulting structural challenges remain a focal point in bridge engineering research [1, 2].

Despite the considerable advancements in materials and design techniques that have driven the evolution of cable-stayed bridges, these structures remain susceptible to significant vibrations induced by environmental factors, such as wind and seismic activity, as well as vehicular loads [3–6]. The intricate dynamic interactions between the cables and beams often exacerbate these vibrations, leading to complex oscillatory behaviors that are challenging to predict and control. This issue has been a persistent challenge in the field of bridge engineering, prompting ongoing research into effective vibration mitigation strategies. Therefore, understanding the coupled dynamics of cable-stayed beams is crucial for developing these strategies [7–9].

Therefore, investigating the coupled dynamics of cable-stayed beams can deepen the understanding of the complex vibration characteristics of cable-stayed bridges. Furthermore, understanding these dynamics provides a foundation for studying internal resonance phenomena, which play a critical role in nonlinear interactions. From this perspective, a series of theoretical and experimental studies on the dynamics of cable-stayed beams has been conducted in recent years. Warnitchai et al.[10] established a Ritz model of a cable-stayed beam using Lagrange's equations. Gattulli et al.[11] derived a continuous system model of a cable-stayed beam using Hamilton's variational principle. Cong et al.[12] studied the modeling, dynamics, and parametric vibration of multi-cable-stayed beams. Su et al.[13] conducted a dynamic analysis of the in-plane free vibration of multi-cable-stayed beams using the transfer matrix method. Wang et al.[14] advanced the theoretical modeling of cable-stayed beam dynamics and studied the impact of cable-beam

*Corresponding author
pengjian@hnu.edu.cn (J. Peng); Lhwang@hnu.edu.cn (L. Wang)

interactions on the natural frequencies of cable-stayed beams. Recently, Kang et al.[15] conducted a nonlinear analysis of cable-beam model of cable-stayed bridges by using the exact mode superposition method and thecable-beam dragging method.

On the other hand, due to the interactions between structural components and the existence of modal couplin[16, 17], the study of internal resonance in cable-beam structures is crucial for understanding the complex nonlinear interactions between different vibration modes. Therefore, the resonance dynamics and nonlinear responses of cable-beam structures have become a key focus of academic research, with many scholars conducting extensive and in-depth studies on this topic. Specifically, Fujino et al. [18] explored multiple internal resonance responses of cable-stayed beams, providing foundational insights into these complex interactions. Xia and Fujino [19] used a three-degree-of-freedom model to investigate the stochastic response of cable-stayed beams, highlighting the importance of considering stochastic excitations in dynamic analysis. Wang et al. [20] studied the 1:1 internal resonance response of cable-stayed beams in the frequency tuning region, demonstrating how specific frequency ratios can enhance modal interactions. Gattulli and colleagues [21, 22] investigated the modal interactions caused by 2:1 internal resonance in cable-stayed beams. They validated their findings with finite element analysis and experiments, emphasizing the importance of these resonances in practical applications. Wei et al. [23] examined the bifurcations and chaos in cable-stayed beams under external excitations, showing the complex dynamic behaviors that can arise in these systems. Cong et al. [24] used the method of multiple scales to study the 2:1 internal resonance of a cable-stayed beam under point excitation, providing a detailed mathematical framework for analyzing these interactions. These nonlinear resonance phenomena can significantly amplify the system's response, leading to large amplitude oscillations, which may potentially impact the structural integrity and performance. These insights have driven extensive research, yet challenges remain in fully capturing the complex dynamics involved.

Overall, while the current research offers valuable insights, it relies on certain assumptions and overlooks some factors, which results in a limited understanding of the full spectrum of dynamic behaviors in cable-stayed beams. For instance, the studies do not fully depict the complex interactions and nonlinear dynamic behaviors that are typical in actual bridge engineering scenarios. Furthermore, the impact of cable-beam interactions during discretization necessitates additional scrutiny, as the static configuration of the cables can significantly influence the beam's dynamic response. Areas such as the interactions between multiple modes, the beam's nonlinear characteristics, and the detailed influence of the cable's static configuration on dynamic response require deeper exploration. To achieve a more accurate and comprehensive understanding of the system's behavior under various excitations, a comprehensive model that captures these complexities is essential.

The main objective of this study was to describe and examine the precise multi-modal discrete model for cable-stayed beam, describing the dynamics of large-amplitude vibrations. The novelty and the main contribution of this work is that it investigates the chaotic dynamics and bifurcation behaviors in cable-stayed beam are investigated through both theoretical analysis and experimental validation, revealing intricate nonlinear responses. Then the complex interactions in cable-stayed beams driven by 2:1 internal resonance under principal resonance conditions are revealed.

The organization of the paper is as follows: in Section 2, a precise multi-modal discrete model for cable-stayed beam is developed using the Hamilton variational principle. Then, perturbation analysis is performed using the method of multiple scales, resulting in the averaged equations and second-order approximate expressions for the nonlinear response under principal resonance in Section 3. Sections 4 tilize numerical results to explore the nonlinear response of the cable-beam. Section 5 establishes an experimental model of the cable-stayed beam to verify the resonance response under 2:1 internal resonance. Discussions and conclusions are presented in Sections 6 and 7.

2. Theoretical model

Consider a cable-stayed beam structure composed of a cantilever beam of length l_b and inclined cables with an angle θ, as illustrated in Fig.1. Two independent Cartesian coordinate systems ($O_c - x_c y_c, O_b - x_b y_b$) are chosen to describe the motion of the cables and the beam separately. The strain in the cables is denoted as $\varepsilon_c(x_c, t) = u_{c,x_c} + y_{c,x_c} v_{c,x_c} + (u_{x_c}^2 + v_{x_c}^2)/2$, where $(\cdot)_{,x_c} = \partial(\cdot)/\partial x_c$; $u_c(x_c, t)$, and $v_c(x_c, t)$ are the axial and in-plane displacement components of the inclined cables, and $y(x_c) = m_c g l_c \cos\theta/(2H_c) x_c(l_c - x_c)[1 - \varepsilon^*(1 - 2x_c)]$ represents the initial configuration of the cables. For the cables, $f = b_c/l_c << 1/8$, where b_c is is the cable sag and $l_c = l_b/\cos\theta$ is the cable span.

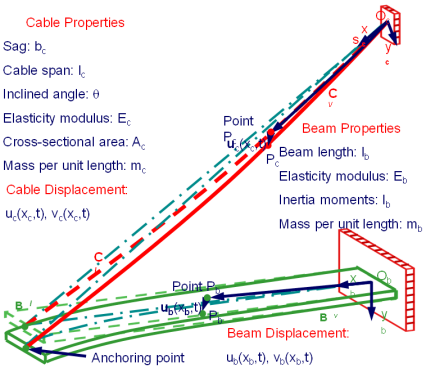

Figure 1: The planar model of the cable-stayed beam and corresponding coordinate systems

2.1. Variational equation

The motion equations and equilibrium conditions for the cable-stayed beam are obtained through the extended Hamiltonian's principle:

$$\delta \int_{t_1}^{t_2} (T - U)dt + \int_{t_1}^{t_2} \delta W dt = 0, \tag{1}$$

where T and U are the kinetic, energy potential of the cable-stayed beam, respectively. δW represents the virtual work done by non-conservative forces, given by:

$$T = \sum\nolimits_{i=b,c} \int_0^{l_i} m_i(\dot{u}_i^2 + \dot{v}_i^2)/2dx_i, \tag{2}$$

$$U = \sum\nolimits_{i=b,c} U_i^I + \sum\nolimits_{i=b,c} \int_0^{l_i} [N_i\varepsilon_i(x_i,t) + E_iA_i\varepsilon_i^2(x_i,t)/2]dx + \int_0^{l_b} E_bI_bv_{b,x_b}^2 dx_b, \tag{3}$$

$$\begin{aligned}\delta W = &\sum\nolimits_{i=b,c} \int_0^{l_i} m_i(\dot{u}_i^2 + \dot{v}_i^2)/2dx_i + \int_0^{l_i} (m_cg\sin\theta\delta u_c + mc_g\cos\theta\delta v_c)dx_c \\ &+ \sum\nolimits_{i=b,c} \int_0^{l_i} [(p_u^i - c_u^i\dot{u}_i)\delta u_i + (p_v^i - c_v^i\dot{u}_i)\delta v_i]dx_i\end{aligned} \tag{4}$$

where one point represents the differential of time t; $m_{b(c)}$ is the mass per unit length of the beam (or cable); $E_{b(c)}$ is the elastic modulus of the beam (or cable); $A_{b(c)}$ is the cross-sectional area of the beam (or cable); $N_c = H$ is the axial component of tension of the cable; $N_b = \int_{A_b} E_b\varepsilon_b^I dA_b$ is the axial force of the beam; ε_b^I is the initial strain of the beam; $I_b = \int_{A_b} y_b^2 dA_b$ is the moment of inertia of the beam's cross-section; $c_{u,v}^{b(c)}$ is the viscous damping coefficient for the beam (or cable); $p_{u,v}^{b(c)}$ is the external load on the beam (or cable).

2.2. Equations of motion

By substituting the Eqs.(2-4) into Eq.(1), and subsequently performing variational operations, the resulting integral terms from the variational process yield the motion equations for the cable-stayed beam

Stay cable:

$$\begin{cases} m_c\ddot{u}_c + c_u^c\dot{u}_c - [E_cA_c\varepsilon_c(x_c,t)]_{,x_c} = p_u^c(x_c,t), \\ v_c\ddot{v}_c + c_u^c\dot{v}_c - [Hv_{c,x_c} + E_cA_c(y_{c,x_c} + v_{c,x_c})\varepsilon_c(x_c,t)]_{,x_c} = p_v^x(x_c,t), \end{cases} \tag{5}$$

Cantilever beam:

$$\begin{cases} m_b\ddot{u}_b + c_u^b\dot{u}_b - [E_bA_b\varepsilon_b(x_b,t)]_{,x_b} = p_u^b(x_b,t), \\ m_b\ddot{v}_b + c_v^b\dot{v}_b + E_bI_bv_{b,x_bx_bx_bx_b} - N_bv_{b,x_bx_b} - [E_bA_bv_{b,x_b}\varepsilon_b(x_b,t)]_{,x_b} = p_v^b(x_b,t), \end{cases} \tag{6}$$

considering the following assumptions: (i) the axial displacement gradients $u_{c,x_c} << 1$ and $u_{b,x_b} << 1$; (ii) neglecting the initial strains in both the cables and the beam. To establish the mechanical and geometric conditions of the cable-stayed beam, the continuity of the displacement field at the anchor points of the cables is taken into account: $\delta\mathbf{u}_b\big|_{x_b=l_b} = R\,\delta\mathbf{u}_c\big|_{x_c=l_c}$, where $\delta\mathbf{u}_b = \{\delta u_b, \delta v_b\}^{\mathrm{T}}, \delta\mathbf{u}_c = \{\delta u_c, \delta v_c\}^{\mathrm{T}}$, $\mathbf{R}$ is the transformation matrix. Clearly, on the one hand, utilizing this condition allows for the derivation of the displacement continuity condition (geometric condition) for the cable-stayed beam:

$$\begin{cases} u_c(l_c,t)\cos\theta - v_c(l_c,t)\sin\theta = u_b(l_b,t), \\ u_c(l_c,t)\sin\theta + v_c(l_c,t)\cos\theta = v_b(l_b,t). \end{cases} \tag{7}$$

On the other hand, incorporating this continuity condition into the partial integration terms yields the continuity condition for the forces in the cable-stayed beam (mechanical condition):

$$\begin{cases} E_bA_b\varepsilon_b|_{x_b=l_b} + E_cA_c\varepsilon_c\cos\theta|_{x_c=l_c} - Hv_{c,x_c}\sin\theta|_{x_c=l_c} - E_cA_c\varepsilon_c(y_{c,x_c}+v_{c,x_c})\sin\theta|_{x_c=l_c} = 0, \\ -E_bI_bv_{b,x_bx_bx_b}|_{x_b=l_b} + E_cA_c\varepsilon_c\sin\theta|_{x_c=l_c} + (N_b + E_bA_b\varepsilon_b)v_{b,x_b}|_{x_b=l_b} \\ +[Hv_{c,x_c} + E_cA_c\varepsilon_c(y_{c,x_c}+v_{c,x_c})]\cos\theta|_{x_c=l_c} = 0, \end{cases} \tag{8}$$

$$E_bI_bv_{b,x_bx_b}|_{x_b=l_b} = 0, \tag{9}$$

where the above expression utilizes the boundary conditions:$u_c(0,t) = 0, v_c(0,t) = 0, u_b(0,t) = 0, v_b(0,t) = 0, v_{b,x_b}(0,t) = 0$.

2.3. Reduced model

For one-dimensional structures, the longitudinal frequency of the structure is significantly greater than the transverse frequency. Therefore, a quasi-static assumption for the structure's motion can be employed. Building upon this, non-dimensional quantities are introduced:

$$\hat{x}_i = x_i/l_i, \hat{v}_i = v_i/l_i, \hat{w}_i = w_i/l_i, i = b,c, \hat{t} = t/l_c\sqrt{H/m_c}. \tag{10}$$

Substituting these into the equations yields the dimensionless motion equations for the cable-stayed beam:

$$\begin{cases} \ddot{v}_c + c_v^c\dot{v}_c - v_{cx_cx_c} - \alpha(y_{cx_cx_c} + v_{cx_cx_c})e_c(t) = p_v^c, \\ \ddot{v}_b + c_v^b\dot{v}_b - Pv_{bx_bx_b} + \beta v_{bx_bx_bx_bx_b} - \Xi v_{bx_bx_b}e_b(t) = p_v^b, \end{cases} \tag{11}$$

where, $\hat{c}_v^c = c_v^cl_c/m_i\sqrt{m_c/H}$, $\hat{y_c} = y_c/l_c$, $\hat{p}_v^i = p_v^im_cl_c^2/(m_ilH)$, $m = m_c/m_b$, $P = m/\cos\theta$, $\alpha = E_cA_c/H$, $\Xi = mE_bA_b/(2H\cos^2\theta)$, $e_c(t) = v_b(1,t)\sin\theta\cos\theta + \int_0^1(y_{c,x_c}v_{c,x_c} + v_{c,x_c}^2/2)d_{x_c}$, $e_b(t) = \int_0^1(v_{b,x_b}^2/2)d_{x_b}$, $\beta = mE_bI_b/(Hl_b^2\cos^2\theta)$.

Simultaneously, the dimensionless boundary conditions can be written as:

$$v_c(0,t) = 0, v_b(0,t) = 0, v_{bx_b}(0,t) = 0, \tag{12}$$

The continuity condition can be expressed as:

$$\begin{cases} v_c(1,t) = v_b(1,t)\cos^2\theta, v_{b,x_bx_b}(1,t) = 0, \\ -\alpha\eta Kv_{b,x_bx_bx_bx_b}(1) + \alpha e_c(t)\sin\theta + v_{c,x_c}(1)\cos\theta \\ -[\cos\theta - \alpha\kappa e_b(t)]v_{b,x_b}(1) + \alpha e_c(t)(y_{c,x_c}(1) + v_{c,x_c}(1))\cos\theta = 0, \end{cases} \tag{13}$$

where $K = E_bI_b/(E_cA_c^2)$; $\eta = A_c/l_b^2$; $\kappa = E_bA_b/E_cA_c$.

2.4. Discrete model

To establish the discrete model of the cable-stayed beam, the displacement $\mathbf{v} = \{v_c, v_b\}^{\mathrm{T}}$ is expanded as:

$$\mathbf{v} = \sum_{r=1}^{\infty} q_r(t)\phi_r, \tag{14}$$

where q_r is the generalized coordinate, ϕ_r represents the r-th mode shape of the cable-stayed beam with a corresponding natural frequency ω_r (refer to references [14, 20] for mode shapes and natural frequencies). In theory, substituting this expression into the motion equation and performing Galerkin integration yields the corresponding discrete model. However, this combined structure includes two distinct structural components, and, more importantly, the mechanical conditions still incorporate the relevant nonlinearity. To address this, the motion equations and mechanical conditions are transformed into the following functionals:

$$\begin{aligned}
&\int_0^1[\ddot{v}_c + c_v^c\dot{v}_c - v_{c,x_cx_c} - \alpha(y_{c,x_cx_c} + v_{c,x_cx_c})e_c(t) - p_v^c]\delta v_c \mathrm{d}x_c + \frac{\cos^3\theta}{m}\int_0^1[\ddot{v}_b + c_v^b\dot{v}_b - Pv_{b,x_bx_b} \\
&+ \beta v_{b,x_bx_bx_bx_b} - \Xi v_{b,x_bx_b}e_b(t) - p_v^b]\delta v_b \mathrm{d}x_b - \cos\theta\{\alpha\eta K v_{b,x_bx_bx_b} - \alpha e_c(t)\sin\theta \\
&+ [\cos\theta - \alpha\kappa e_b(t)]v_{b,x_b} - v_{c,x_c}\cos\theta - \alpha e_c(t)(y_{c,x_c} + v_{c,x_c})\cos\theta\}\delta v_b|_{x_b=1} = 0.
\end{aligned} \tag{15}$$

Substituting the displacement expansion into Eq.(15) and utilizing the stationary value condition of the functional yields:

$$\ddot{q}_k + 2\mu_k\dot{q}_k + \omega_k^2 q_k = \sum_{i=1}^{\infty}\sum_{j=1}^{\infty}\Lambda_{kij}q_iq_j + \sum_{i=1}^{\infty}\sum_{j=1}^{\infty}\sum_{h=1}^{\infty}\Gamma_{kijh}q_iq_jq_h + f_k\cos\Omega t, k = 1, 2, \cdots, \infty \tag{16}$$

Here, the expression considers the orthogonality and orthogonal damping between modes, while the coefficient expressions can be found in references [14, 20].

3. Perturbation analysis

To investigate the nonlinear modal interactions of the cable-stayed beam, the motion equations are transformed into state-space (first-order) form:

$$\begin{cases}
\dot{q}_k - z_k = 0, \\
\dot{z}_k + 2\mu_k z_k + \omega_k^2 q_k = \sum\limits_{i=1}^{\infty}\sum\limits_{j=1}^{\infty}\Lambda_{kij}q_iq_j + \sum\limits_{i=1}^{\infty}\sum\limits_{j=1}^{\infty}\sum\limits_{h=1}^{\infty}\Gamma_{kijh}q_iq_jq_h + f_k\cos\Omega t.
\end{cases} \tag{17}$$

For weakly nonlinear problems, the method of multiple scales is employed to determine the second-order approximate solution for the cable-stayed beam. The parameters μ_k and f_k are adjust to be $\varepsilon^2\mu_k$ and $\varepsilon^2 f_k$, ε are non-dimensional small parameters. Next, assume that the generalized coordinate forms for displacement and velocity can be expanded as $q_k\big|\, z_k(t;\varepsilon) = \sum_{i=1}^{3}\varepsilon^i q_{ki}\big|z_{ki}(T_0, T_1, T_2) + \cdots$, where the time scale T_k is defined as $T_k = \varepsilon^k t(k = 0, 1, 2)$. Therefore, the derivative with respect to time t can be defined as $\partial/\partial T$. Additionally, to account for internal resonances and primary resonance between different modes, introduce tuning parameters σ_1 and σ_2 such that they satisfy $\omega_n = 2\omega_m + \varepsilon\sigma_1$ and $\Omega = \sum_{j=1}^{2}\delta_{ij}\omega_j + \varepsilon\sigma_2$, where δ_{ij} is the Kronecker delta function. Following the steps provided by the method of multiple scales[25, 26], the averaged equations for the 2:1 internal resonance of the cable-stayed beam can be obtained:

$$2\mathrm{i}\omega_m(\mu_m A_m + D_2 A_m) = S_{mm}A_m^2\bar{A}_m + S_{mn}A_mA_n\bar{A}_n + \frac{f_m}{2}\delta_{mi}\mathrm{e}^{\mathrm{i}\varepsilon^2\sigma_2T_2}, \tag{18}$$

$$2\mathrm{i}\omega_n(\mu_n A_n + D_2 A_n) = S_{nn}A_n^n\bar{A}_n + S_{nm}A_m\bar{A}_mA_n + \frac{f_n}{2}\delta_{ni}\mathrm{e}^{\mathrm{i}\varepsilon^2\sigma_2T_2}, \tag{19}$$

where A_m and A_n are the complex amplitude values for the first and second-order modes, and $S_i(S_{ij})$ are the first (second) order nonlinear coefficients [25]. Overall, these coefficients account for the influences of both resonant and non-resonant modes. For the primary resonance case, polar coordinate transformations $A_j = 1/2a_j e^{i\beta_j}(j = 1, 2)$, where a_j and β_j are the amplitude and phase of the j-th mode, respectively. These transformations are then substituted into Eq.(18) and Eq.(19). By separating the real and imaginary parts, the polar coordinate form corresponding to the averaged equations is obtained.

$$8\omega_m \dot{a}_m = -8\mu_m a_m \omega_m + 2S_m a_m a_n \sin\gamma_1 + 4f_m \delta_{mi} \sin\gamma_2 \tag{20}$$

$$-8\omega_1 a_1 \dot{\beta}_1 = 2S_m a_m a_n \cos\gamma_1 + S_{mm} a_m^3 + S_{mn} a_m a_n^2 + 4f_m \delta_{mi} \cos\gamma_2 \tag{21}$$

$$8\omega_n \dot{a}_n = -8\mu_n a_n \omega_n - 2S_n a_n^2 \sin\gamma_1 + 4f_m \delta_{ni} \sin\gamma_3 \tag{22}$$

$$-8\omega_n a_n \dot{\beta}_n = 2S_n a_n^2 \cos\gamma_1 + S_{nn} a_n^3 + S_{nm} a_m^2 a_n + 4f_m \delta_{ni} \cos\gamma_3 \tag{23}$$

where,$\gamma_1 = \sigma_1 t - 2\beta_m + \beta_n, \gamma_2 = \sigma_2 t - \beta_n, \gamma_3 = \sigma_2 t - \beta_m$.

The second-order expansion for displacement is as follows:

$$\begin{aligned} v(x,t) = {} & a_m \cos(\omega_m t + \beta_m)\phi_m(x) + a_n \cos(\omega_n t + \beta_n)\phi_n(x) + \frac{1}{2}\{a_m^2[\cos 2(\omega_m t + \beta_m)\psi_{mm}(x) \\ & + \kappa_{mm}(x)] + a_n^2[\cos 2(\omega_n t + \beta_n)\psi_{nn}(x) + \kappa_{nn}(x)] + a_m a_n[\cos(\omega_m t + \omega_n t + \beta_m + \beta_n)\psi_{mn}(x) \\ & + \cos(\omega_m t - \omega_n t + \beta_m - \beta_n)\kappa_{mn}(x)]\}, \end{aligned} \tag{24}$$

where,

$$\begin{aligned} \psi_{mm}(x) &= \sum_{k=1,k\neq n}^{\infty} \frac{\Lambda_{kmm}}{\omega_k^2 - 4\omega_m^2}\phi_k(x) + \frac{\Lambda_{nmm}}{4\omega_n^2}\phi_n(x); \\ \kappa_{mn}(x) &= \sum_{k=1,k\neq m}^{\infty} \frac{\Lambda_{kmn} + \Lambda_{knm}}{\omega_k^2 - (\omega_m - \omega_n)^2}\phi_k(x) + \frac{\Lambda_{mmn} + \Lambda_{mnm}}{4\omega_m^2}\phi_m(x); \psi_{nn}(x) = \sum_{k=1}^{\infty} \frac{\Lambda_{knn}}{\omega_k^2 - 4\omega_n^2}\phi_k(x); \\ \psi_{mn}(x) &= \sum_{k=1}^{\infty} \frac{\Lambda_{kmn} + \Lambda_{knm}}{\omega_k^2 - (\omega_m + \omega_n)^2}\phi_k(x); \kappa_{mm}(x) = \sum_{k=1}^{\infty} \frac{\Lambda_{kmm}}{\omega_k^2}\phi_k(x); \kappa_{nn}(x) = \sum_{k=1}^{\infty} \frac{\Lambda_{knn}}{\omega_k^2}\phi_k(x). \end{aligned} \tag{25}$$

Overall, the equilibrium solutions of the averaged equations correspond to periodic motion of the cable-stayed beam. To determine the equilibrium solutions of the averaged equations, one can set $\dot{a}_k = \dot{\gamma}_k = 0(k = m, n)$ in the equations, and then apply the Newton-Raphson method to solve the nonlinear equations. Additionally, by setting the mixed terms involving a_m and a_n, as well as $\sigma_1 = 0$, in Eqs.(20)-(23) to 0, the nonlinear single-mode solution without considering internal resonance can be obtained, where the amplitude $a_k(k = m, n)$ satisfies

$$K_{kk}^2 a_k^6 + 16\omega_k \sigma_2 a_k^4 + [(8\mu\omega_k)^2 - 64\omega_k^2 \sigma_2)^2]a_k^2 - (4f_k)^2 = 0 \tag{26}$$

It is apparent that the averaged equations only admit bi-modal solutions: (i) Single-mode solution: $a_1 = 0, a_2 \neq 0$; (ii) Two-mode solution: $a_1 \neq 0, a_2 \neq 0$. For the former, it is possible to obtain:

$$K_{nn}^2 a_n^6 - 16\omega_n(\sigma_1 - \sigma_2)a_n^4 + [(8\mu\omega_n)^2 + 64\omega_n^2(\sigma_1 - \sigma_2))^2]a_n^2 - (4f_k)^2 = 0 \tag{27}$$

Here, the single-mode solution is influenced by another internally resonant mode (σ_1). This influence results in differences in both the magnitude and stability of the solution compared to the single-mode solution without

considering internal resonance, particularly in terms of stability. The critical stability point of the single-mode solution that accounts for internal resonance is likely a pitchfork bifurcation point where it intersects with the multi-mode solution.

To determine the stability of the equilibrium solutions, a Cartesian transformation $A_k(t) = \frac{1}{2}[p_k(t) - \mathrm{i}q_k(t)]\mathrm{e}^{\mathrm{i}\beta_k}$, $k = m, n$ is introduced and the real and imaginary parts are separated. Based on this, the Cartesian form of the averaged equations can be obtained

$$\dot{p}_m = -\mu_m p_m - \kappa_m q_m - \frac{K_{mm}}{8\omega_m} q_m(p_m^2 + q_m^2) - \frac{K_{mn}}{8\omega_m} q_m(p_n^2 + q_n^2) + \frac{K_m}{4\omega_m}(q_m p_n - p_m q_n) \tag{28}$$

$$\dot{q}_m = -\mu_m q_m + \kappa_m p_m + \frac{K_{mm}}{8\omega_m} p_m(p_m^2 + q_m^2) + \frac{K_{mn}}{8\omega_m} p_m(p_n^2 + q_n^2) + \frac{K_m}{4\omega_m}(p_m p_n + q_m q_n) + \frac{f_m}{2\omega_m}\delta_{mi} \tag{29}$$

$$\dot{p}_n = -\mu_n p_n - \kappa_n q_n - \frac{K_{nn}}{8\omega_n} q_n(p_n^2 + q_n^2) - \frac{K_{nm}}{8\omega_n} q_n(p_m^2 + q_m^2) + \frac{2K_n}{4\omega_n} p_m q_m \tag{30}$$

$$\dot{q}_n = -\mu_n q_n + \kappa_n p_n + \frac{K_{nn}}{8\omega_n} p_n(p_n^2 + q_n^2) + \frac{K_{nm}}{8\omega_n} p_n(p_m^2 + q_m^2) + \frac{K_n}{4\omega_n}(p_m^2 - q_m^2) + \frac{f_n}{2\omega_n}\delta_{ni} \tag{31}$$

Specifically, when $\Omega \approx \omega_m$ occurs: $\kappa_m = \sigma_2$, $\kappa_n = 2\sigma_2 - \sigma_1$; when $\Omega \approx \omega_n$ occurs: $\kappa_m = \sigma_1 + \sigma_2$, $\kappa_n = (\sigma_1 + \sigma_2)/2$. Furthermore, the amplitude of the system's response can be obtained

$$a_m = \sqrt{p_m^2 + q_m^2}, a_n = \sqrt{p_n^2 + q_n^2}. \tag{32}$$

4. Two-to-one internal resonance response

Next, to study the 2:1 internal resonance response of the cable-stayed beam, we select the geometric parameters from [20].Based on these parameters, the in-plane natural frequencies of the inclined cable-stayed beam can be numerically determined using the frequency characteristic equation, as illustrated in Fig.2. It can be observed that

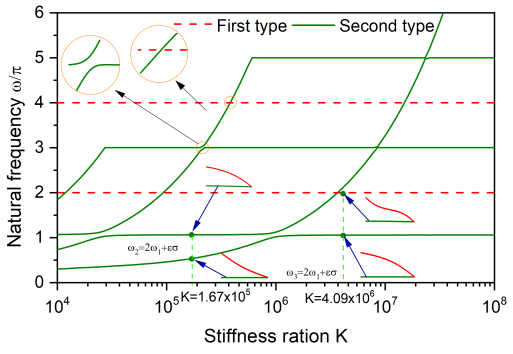

Figure 2: Frequency spectrum of the cable-stayed beam, with mode shapes involved in 2:1 internal resonances

at $K = 1.67 \times 10^5$ and $K = 4.09 \times 10^6$, the first-order natural frequency respectively shows $\omega_n \approx 2\omega_m$ with the second/third-order natural frequencies, hence the 2:1 internal resonance between the beam modes might be excited. On the other hand, the nonlinear coefficients exhibit good convergence, and the influence of all non-resonant modes on the nonlinear coefficients is minor. Therefore, the first ten modes are selected to determine the nonlinear coefficients of the averaged equations (see in Tab.1). Clearly, the nonlinear coefficients S_m and S_n are non-zero, thus the 2:1 internal resonance of the cable-stayed beam can be excited. Additionally, in the subsequent numerical studies, a relatively small excitation amplitude ($f_i = 0.0001$,i=1,2,3) and a viscous damping coefficient ($\mu_i = 0.001$) are chosen.

Table 1
Parameters of the cable-stayd beam and effective nonlinear coefficients of the modulation equations

Case	$K\times10^5$	Mode		Natural Frequency		Effective Nonlinear Coefficient						ω_m:ω_n
		m	n	ω_m	ω_n	S_{mm}	S_{mn}	S_{nn}	S_{nm}	S_m	S_n	
I	1.67	1	2	1.6743	3.3419	827.77	4324.06	36075.7	59175.4	16.3	288	**Global: Local**
II	40.9	1	3	3.3219	6.6376	-36812	-128070	-145.47	-2141.6	4.81	-1.51	**Local: Global**

4.1. Case I ($K = 1.67 \times 10^5$)

Firstly, the dimensionless stiffness ratio $K = 1.67 \times 10^5$ is selected, where the internal resonance modes of the cable occur between the first and second order modes($\omega_1 : \omega_2 = 1.6743 : 3.3419$), specifically, global modal: local modal exhibiting a 2:1 internal resonance.

Fig.3(a) shows the frequency-response curves of the cable-stayed beam during the primary resonance of the first-order mode ($\Omega \approx \omega_1$). Solid lines indicate stable solutions, and dashed lines represent unstable solutions. Circles and plus signs denote the numerical integration solutions of the direct solution. The results show that the numerical integration solutions are in good agreement with the regimen solutions obtained by the multiscale method. SN and HB represent the saddle-node and HB points, respectively. The frequency-response curves of the cable-stayed beam exhibits distinct nonlinear characteristics and a multivalued region, with only bi-modal solutions present. Due to the effective nonlinear coefficient S_{11} being greater than zero, when the tuning parameter σ_2 is small, the frequency-response curve exhibits a soft spring characteristic. Simultaneously, the amplitudes of directly and indirectly excited modes, a_1 and a_2, decrease as the tuning parameter σ_2 increases. Conversely, when the tuning parameter σ_2 is large, the frequency-response curve includes two unstable solution branches and one stable branch, exhibiting hard spring characteristics. As the tuning parameter σ_2 decreases, one of the unstable solution branches undergoes a Hopf bifurcation at HB1 ($\sigma_2 \approx 0.0118$), leading to the bi-modal solution of the cable-stayed beam. Notably, there is an unstable region between the HB point HB1 and the saddle-node bifurcation point SN3, where the motion of the cable-stayed beam in this frequency region is non-periodic.

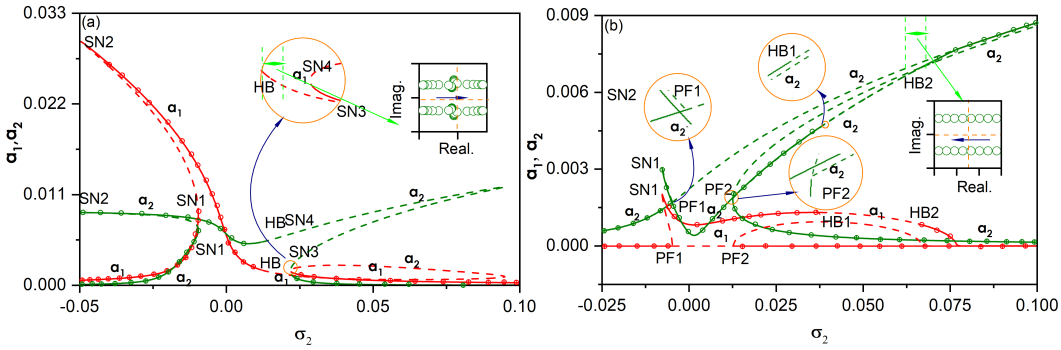

Figure 3: Frequency-response curves of the cable-stayed beam when $K = 1.67 \times 10^5$, (a)$f_1 = 0.0001$, $f_2 = 0$, $\Omega \approx \omega_1$; (b)$f_1 = 0$, $f_2 = 0.0001$, $\Omega \approx \omega_2$. Analytical solution: ——— stable, ····· unstable; numerical solution: ∘ sweep up, + sweep down

Fig.3(b) depicts the frequency-response curves of the cable-stayed beam under the primary resonance of the second modal mode($\Omega \approx \omega_2$). PF denotes the pitchfork bifurcation point. It can be observed that the single-mode solution exhibits a distinct multi-valued region. It loses stability at the pitchfork bifurcation point PF1 but regains stability through another pitchfork bifurcation at PF2. On the other hand, the two-mode solution displays two prominent multi-valued regions. In the left multi-valued region, the indirect excitation mode has a relatively significant impact on the nonlinear response of the cable-stayed beam. However, in the right multi-valued region, the nonlinear response of the cable-stayed beam is controlled by the directly excited mode. Additionally, the two-mode solution branch features two HB points.

Fig.4(a) shows the response curves of the amplitudes of the first and second-order modes as a function of the external excitation amplitude, with the tuning parameter $\sigma_2 = 0.05$. When the excitation amplitude $f_1 \in (0.0000365, 0.00043)$, the two-mode response of the cable-stayed beam has two unstable branches and one stable branch. The stable branch loses stability at the saddle-node bifurcation point SN1 and regains stability at the HB point HB1 as the excitation amplitude increases. Notably, the amplitude of the first-order mode increases linearly with increasing external excitation, while the second-order mode exhibits a relatively significant saturation effect. Clearly, the energy transfer mechanism provided by the 2:1 internal resonance does not enable the cable to gain more energy at this time.

Fig.4(b) presents the force-response curve of the cable-stayed beam under the primary resonance($\Omega \approx \omega_2$) of the second modal mode, where the tuning parameter $\sigma_2 = 0.05$. It can be observed that the single-modal solution loses stability through a subcritical bifurcation at PF1, leading to the appearance of a two-modal solution. Additionally, the single-modal solution regains stability through a saddle-node bifurcation at SN1. As the external excitation amplitude f_2 increases from SN1, there is a noticeable saturation in the amplitude of the directly excited modal mode. Simultaneously, the influence of the indirectly excited modal mode on the nonlinear response of the cable-stayed beam becomes relatively pronounced.

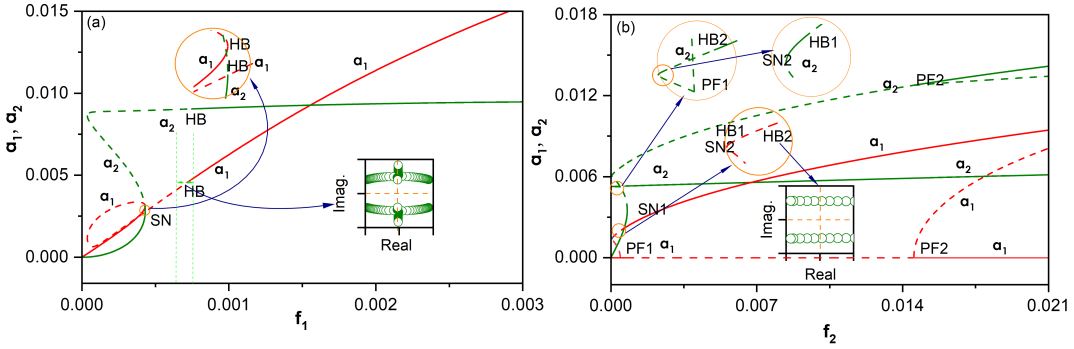

Figure 4: Force-response curves of the cable-stayed beam when $K = 1.67\times10^5$, $\sigma_2 = 0.05$, (a)$f_2 = 0$, $\Omega \approx \omega_1$; (b)$f_1 = 0$, $\Omega \approx \omega_2$

The frequency-response and force-response curves above exhibit HB points. Corresponding to these bifurcations, the averaged equations have periodic solutions with a period of $2\pi/|\beta|$, where β is the imaginary part of the eigenvalues of the Jacobian matrix. To further investigate the nonlinear dynamics of the cable-stayed beam, the shooting method is employed to determine periodic solutions of the averaged equations. Additionally, Floquet theory is used to determine the stability of the periodic solutions. Fig.5a presents the bifurcation diagram of the periodic solutions derived from the HB point in Fig.3(a), where PD denotes the period-doubling bifurcation point. The maximum (minimum) value of the amplitude is denoted as p_1, and solid and hollow circles represent stable and unstable periodic solutions, respectively. It can be seen that stable periodic solutions are derived from HB, indicating that the corresponding Hopf bifurcation is subcritical. As the tuning parameter $\sigma_2 \approx 0.01183$ increases, the stable period-1 solution (P-1) becomes unstable after passing through the period-doubling bifurcation point PD1. With the continuous increase of the tuning parameter, a series of different period-doubling bifurcations occur.

Fig.5b illustrates the periodic solution branch derived from the HB point in Fig.4(a). A stable periodic solution branch originates from the HB. As the excitation amplitude decreases, the amplitude of the periodic solution's limit cycle gradually increases. Beyond PD1, it loses stability and gives rise to another P-2 solution branch (Fig.5b). As the excitation amplitude continues to decrease, the system undergoes a series of period-doubling bifurcations, leading to chaos.

To further illustrate the characteristics of periodic solutions, Fig.6 shows the evolution of the phase plane within this frequency range as the tuning parameter varies. The limit cycle in the phase plane undergoes one closed loop (Fig.6a), two closed loops (Fig.6b), and multiple closed loops (Fig.6c) due to a series of period-doubling bifurcations. Eventually, a chaotic attractor emerges (Fig.6d). Fig.6e and Fig.6f show the FFT and Poincaré section of this attractor,

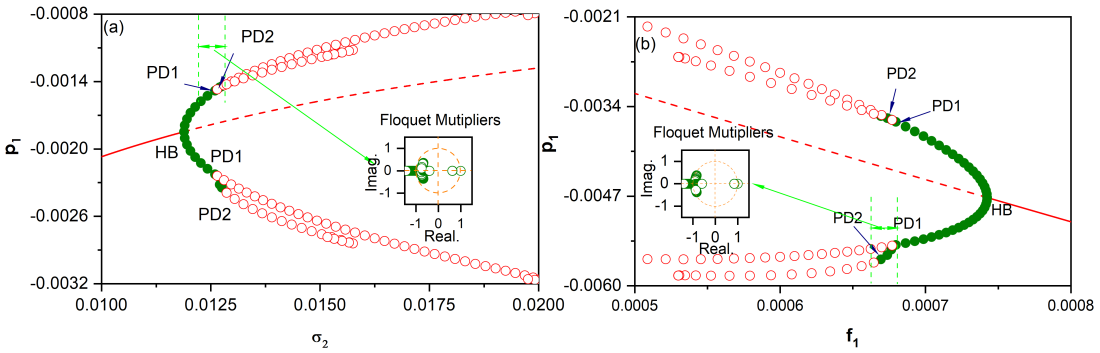

Figure 5: Periodic solution branches when $\Omega \approx \omega_1$, (a)$\sigma_2 \in (0.01183, 0.0199)$; (b)$f_1 \in (0.0005, 0.0008)$

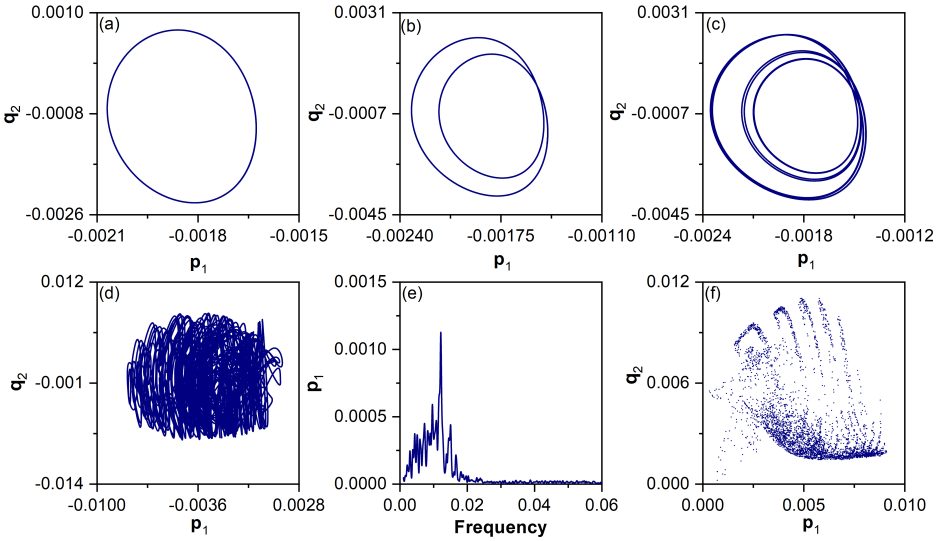

Figure 6: Dynamic solutions of the averaged equations when $\Omega \approx \omega_1$, (a)$\sigma_2 = 0.012136$ (P=1); (b)$\sigma_2 = 0.012716$ (P=2); (c)$\sigma_2 = 0.012769$ (P=8); (d)$\sigma_2 = 0.012776$ (chaotic); (e)$\sigma_2 = 0.012776$ (spectral analysis of chaotic motion); (f)$\sigma_2 = 0.012776$ (Poincaré section of chaotic motion)

respectively. This chaotic attractor exists in a relatively small frequency range. As the tuning parameter continues to increase, the system undergoes a sudden change, leading to additional stable equilibrium solutions.

Fig.7 shows the corresponding change in the period solution branch, where CF denotes the folding bifurcation. This corresponds to the appearance of two HB points (HB1 and HB2) in the bimodal response in Fig.3(b). Between these bifurcation points, the averaged equations may exhibit rich nonlinear dynamics. Stable periodic solutions emerge from HB1, and unstable periodic solutions originate from HB2, indicating that the former is supercritical, while the latter is subcritical. As the tuning parameter σ_2 decreases, the limit cycles of the P-1 solutions, initiated from HB1 and HB2, gradually increase. Eventually, at the fold bifurcation (CF), the stability of the periodic solutions changes, with the former losing stability and the latter gaining stability.

Fig.8a and Fig.8b depict the two periodic solution branches derived from the Hopf bifurcations at HB1 and HB2 in Fig. 8. A subcritical Hopf bifurcation at HB1 generates an unstable periodic solution branch (Fig.8a), while a supercritical Hopf bifurcation at HB2 gives rise to an unstable periodic solution branch (Fig.8b). As the excitation

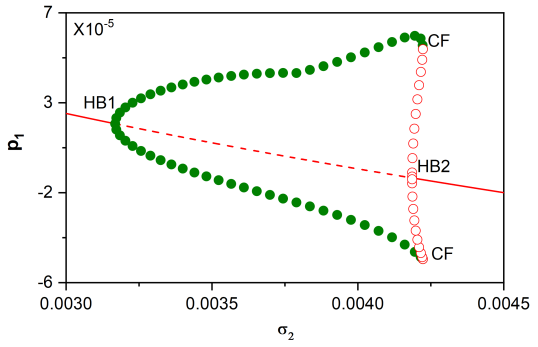

Figure 7: Periodic solution branches when $\Omega \approx \omega_2$, $\sigma_2 \in (0.0030, 0.0045)$

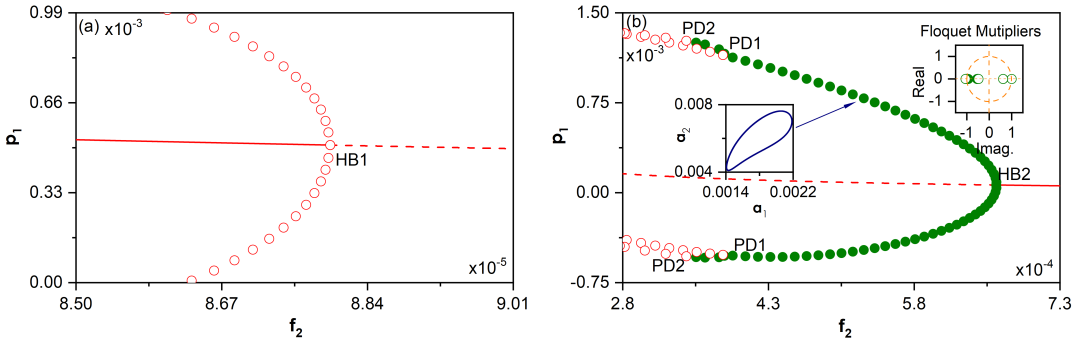

Figure 8: Periodic solution branches when $\Omega \approx \omega_2$, (a)$f_2 \in (0.000085, 0.00009)$; (b)$f_2 \in (0.000280, 0.000720)$

amplitude decreases, the limit cycles of the periodic solutions gradually increase. Notably, the stable P-1 solution loses its stability through a period-doubling bifurcation at PD1, while along the P-2 solution branch derived at this point, a series of period-doubling bifurcations can still be observed. When the excitation amplitude is reduced to a specific value, the dynamic solutions of the system exhibit chaotic characteristics, with the periodic solutions becoming chaotic through period-doubling instabilities, as shown in Fig.9.

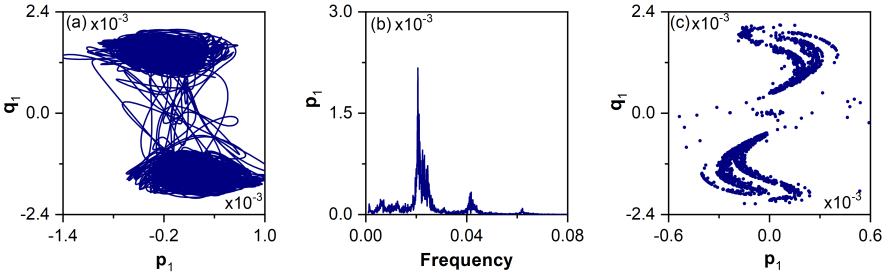

Figure 9: Chaotic motion when $f_2 = 0.000349$, $\Omega \approx \omega_2$, (a) Phase trajectory diagram; (b) Spectral analysis; (c) Poincaré section

4.2. Case II($K = 4.09 \times 10^6$)

Secondly, the dimensionless stiffness ratio $K = 4.09 \times 10^6$ is selected, where the internal resonance modes of the cable occur between the first and third orders($\omega_1 : \omega_3 = 3.3219 : 6.6376$), specifically as local mode: global mode exhibiting a 2:1 internal resonance.

Fig.10(a) shows the frequency-response curves for the primary resonance of the first-order mode. The overall response of the first-order primary resonance is similar to the nonlinear response of the first-order single mode, but during resonance, some energy is transferred to the third-order mode. However, the transferred energy is small, and the third-order mode is only excited to a linear response with small amplitudes, the largest being only $a_3 = 0.000401$. Naturally, due to interaction, the amplitude of the first-order mode changes within the corresponding frequency range. Not only does the magnitude change, but the stability also alters, resulting in two HB points.

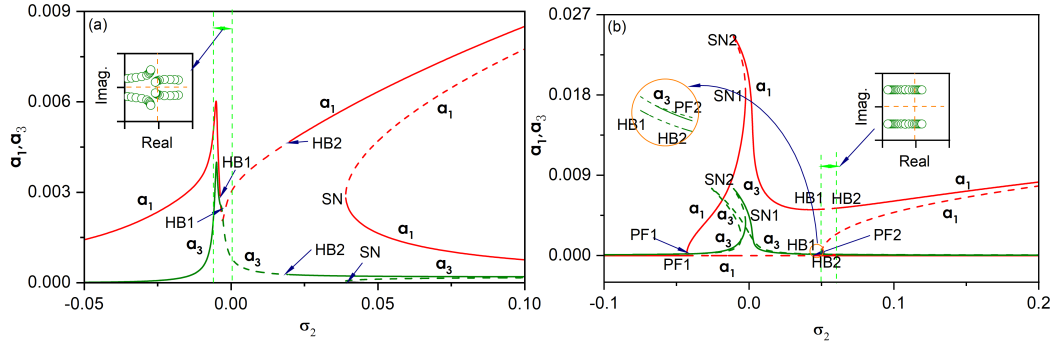

Figure 10: Frequency-response curves of the cable-stayed beam when $K = 4.09 \times 10^6$ (a)$f_1 = 0.0001$, $f_3 = 0$, $\Omega \approx \omega_1$; (b)$f_1 = 0$, $f_3 = 0.0001$, $\Omega \approx \omega_3$

Fig.10(b) shows the frequency-response curves for the third-order primary resonance mode. At this time, the structural resonance response shows great similarity to the resonance of parameters related solely to the cable in support vibrations. The directly excited modes contain components of the beam, and the excitation frequency is approximately twice the fundamental frequency of the pure cable. In the 2:1 internal resonance, high-order energy can easily be transferred to lower orders through self-excited resonance. Due to stiffness differences, small displacements at the beam ends may produce large amplitudes in the cable, suggesting that the resonance response will be very rich. As seen in Fig.10(b), the stable responses of the directly excited modes are primarily linear, with slight curvature in the frequency-response curves and small response amplitudes. However, the amplitudes of responses of indirectly excited local modes are large. Since the single-mode solution becomes unstable between PF1 and PF2, a large-amplitude multi-mode response becomes the most likely form of response. When the excitation frequency exceeds the frequency at point PF2, the single-mode solution regains stability but can still cause large amplitude vibrations in the cable. Unlike before, the responses of global modes are much smaller at this time.

Fig.11(a) shows the response curve of the system's modal response to changes in external excitation during the primary resonance of the first-order mode. Similar to the frequency-response curves, the internal resonance effect is not pronounced. The response curve is similar to that of a typical single-mode nonlinear response, and the response of the indirectly excited modes is minimal.

Fig.11(b) shows the curve of the third-order primary resonance mode response as external excitation changes. The response of the directly excited mixed mode increases linearly with excitation. In contrast, the amplitudes of the indirectly excited local modes are much larger and dominate the structural response

Fig. 12 illustrates the period solution branch between two HB points, corresponding to the case in Fig.10(a). Both HB points are supercritical. The periodic solution branching from the HB1 bifurcation point becomes unstable after a period-doubling bifurcation and jumps to a larger periodic motion upon a slight disturbance (as shown in the time series curve in Fig.12(a)). The periodic solutions branching from the HB2 bifurcation point alternate between stability and instability, maintaining a long stable period as the tuning parameter decreases until near $\sigma_2 = 0.0016$, where the solution transitions from period-doubling to chaos. Fig.13 shows the phase trajectory, spectral analysis, and Poincaré section of chaotic motion at $\sigma_2 = 0.0016$. The range of the chaotic attractor is small, with the maximum response of

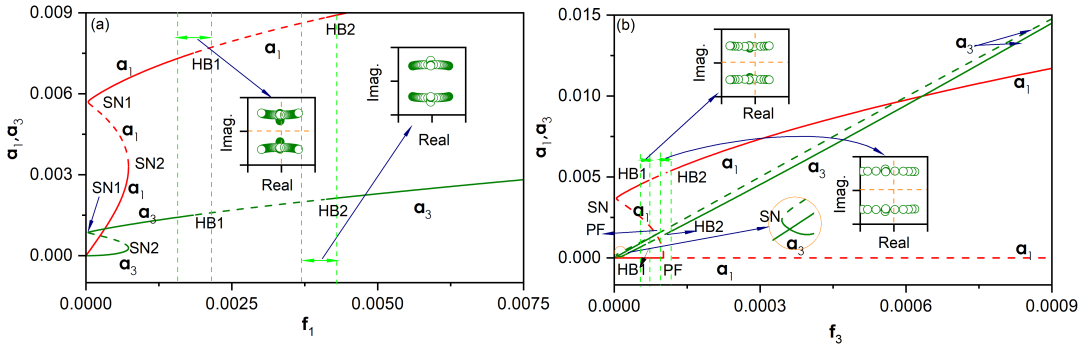

Figure 11: Force-response curves of the cable-stayed beam when $K = 4.09\times10^6$, $\sigma_2 = 0.05$ (a)$f_3 = 0$, $\Omega \approx \omega_1$; (b)$f_1 = 0$, $\Omega \approx \omega_3$

the first-order mode being 0.004, and the third-order mode response being an order of magnitude smaller. Thus, the impact on system safety is minimal. Fig.14 shows the closed mid-range periodic solution branch from Fig.11(a).

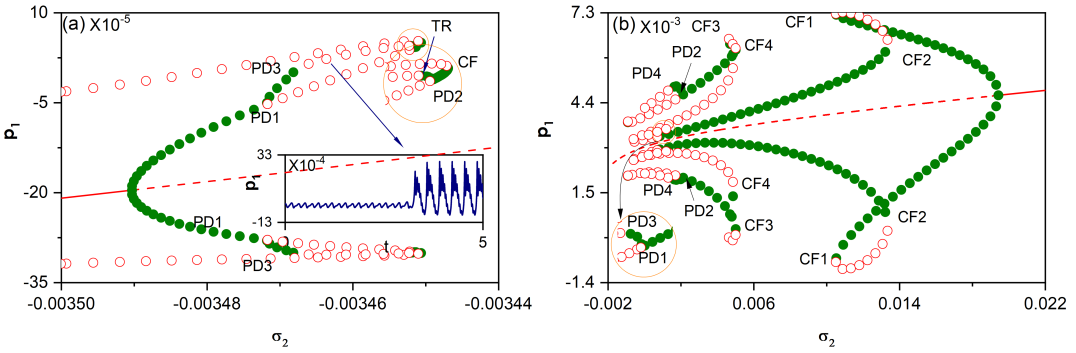

Figure 12: Periodic solution branches when $\Omega \approx \omega_1$, (a) $\sigma_2 \in (-0.000350, -0.000342)$; (b) $\sigma_2 \in (-0.00200, 0.00022)$

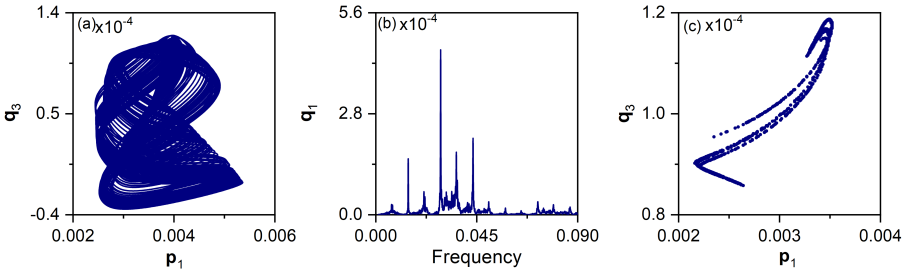

Figure 13: Chaotic motion $\sigma_2 = 0.0015$, $\Omega \approx \omega_1$, (a) Phase trajectory diagram; (b) Spectral analysis; (c) Poincaré section.

Fig.14 and Fig.10(a) show that the excitation acting on the local modes is unlikely to be transmitted to higher-order mixed modes through a 2:1 internal resonance. This can be attributed to several factors: local modes are lower-order, making the flow of energy from lower to higher orders more difficult than from higher to lower orders. Additionally,

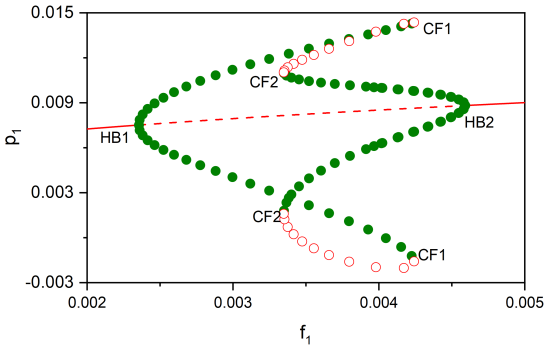

Figure 14: Periodic solution branches when $\Omega \approx \omega_1$, $f_1 \in (0.0020, 0.0050)$

because the mixed modes are antisymmetric modes induced by adjacent local modes, the symmetric modes within the local modes participating in internal resonance are orthogonal, significantly reducing the modal coupling effect produced by nonlinear interactions.

Fig.15(a) shows the periodic solution branches between HB1 and HB2 in Fig.10(b). As illustrated, the periodic solutions between the two HB points are closed, indicating that the structural response between these points cannot be approximated by the support motion. This is because, in forced vibration, the excitation amplitude of the supports is fixed and does not change over time. However, overall, the mixed modes involving beams can experience dynamic instability with local modes, leading to continuous energy exchange. This means that the amplitude of beam vibrations may vary over time.

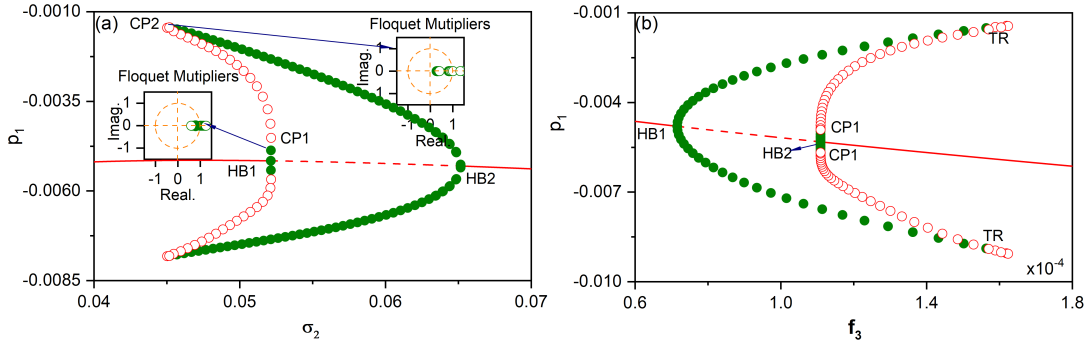

Figure 15: Periodic solution branches when $\Omega \approx \omega_3$ (a)$\sigma_2 \in (0.0400, 0.0700)$; (b)$f_3 \in (0.000060, 0.000018)$

Fig.15(b) illustrates the periodic solution within the HB point shown in Fig.11(b). The curve is relatively simple but still demonstrates the dominant role of the indirectly excited local modes, with the periodic solutions at the HB points shown in Fig.15b. Notably, in the 2:1 internal resonance between mixed and local modes, neither mode shows saturation phenomena during primary resonance. Both modes can absorb energy from the external environment through direct or indirect means, increasing in amplitude with increasing excitation amplitude.

5. Experimental comparison

To validate the accuracy of the cable-stayed beam modeling and the corresponding phenomena, an experimental model of the cable-stayed beam was established in this section to determine the resonance response of the cable-stayed beam under the effect of 2:1 internal resonance.

5.1. Experimental setup

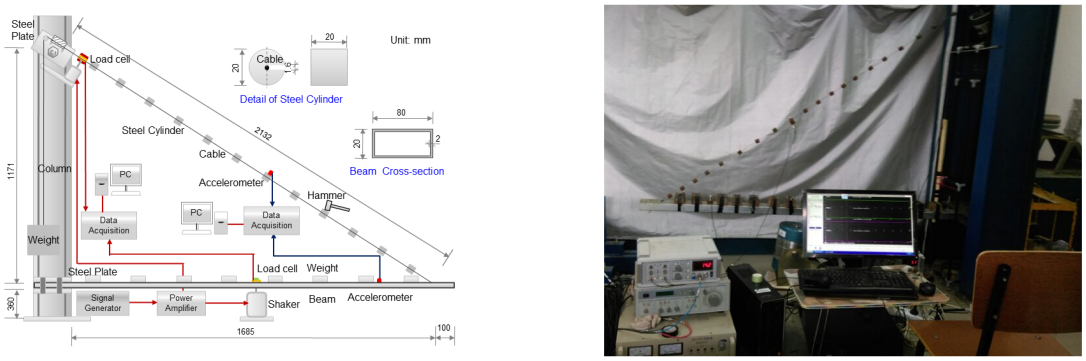

Figure 16: Experimental design diagram and physical model

The experimental design of the cable-beam structural model is shown in the left panel of Fig.16, where the beam is made of an aluminum alloy square tube with an elastic modulus of 28 GPa and a density of 2500 kg/m^3. The dimensions of the beam's cross-section are as illustrated. The moment of inertia for bending along the short edge of the beam is 26.298 cm^4. A counterweight of 1kg is fixed at the designed position to serve as the beam's mass. The right end of the beam is clamped with a steel plate to simulate a fixed-end constraint of a one-dimensional component, while the other end is connected to the cable, leaving 10 cm of length beyond the connection point for placing a centrifuge and sensors.

The cable is made of 1.5 mm diameter 1860 steel strand with an elastic modulus of 200 GPa. One end of the cable is connected to the beam, and the other end passes over a reaction frame to hang a basket (self-weight: 10 kg) for placing weights that generate cable tension. Once the cable tension is determined, the upper end of the cable is clamped to prevent steel wires outside the calculated length from participating in vibrations during testing. Neglecting the self-weight of the steel wire, counterweights are uniformly distributed along the wire as needed. The counterweights are iron cylinders with a diameter of 20 mm and a height of 20 mm, each weighing 0.049 kg. The actual experimental model is shown in the right panel of Fig.16.

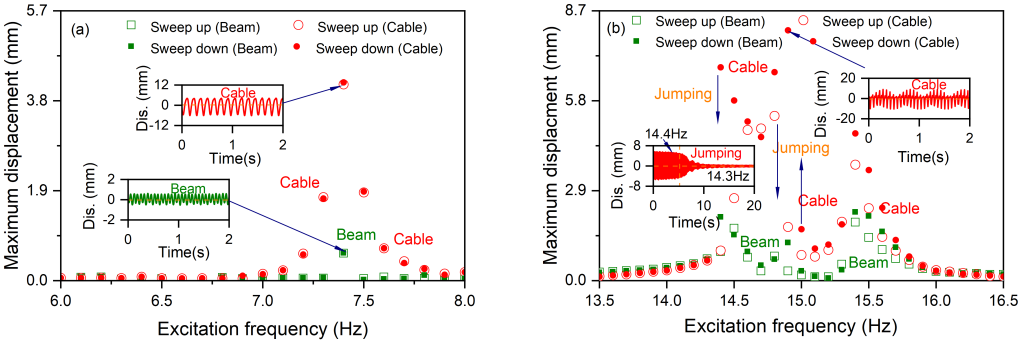

Figure 17: Experimental frequency response diagram, representing the maximum amplitude of oscillations versus frequency, (a)Excitation frequency $\in (6.0, 8.0)$, (b)Excitation frequency $\in (13.5, 16.5)$

5.2. Experimental dynamics at 2:1 internal resonance

To observe the internal resonance response of the cable-beam structure, a small load of 0.5 N is applied at the midpoint of the beam. Experimental results demonstrate the relationship between the external excitation frequency and

Table 2
Coefficients of the tuning equations with and without interactions

Case	$K\times10^5$	ω_m:ω_n	Natural Frequency		Effective Nonlinear Coefficient					
			ω_m	ω_n	S_{mm}	S_{mn}	S_{nn}	S_{nm}	S_m	S_n
With interactions	1.67	Global:Local	1.6743	3.3419	827.77	-4324.06	-36075.7	-59175.4	16.3	288
Without interactions	1.67	Global:Local	1.6743	3.3419	51.33	-1186.6 1	-35303.4	-15701	-10.97	-75.2

maximum displacement processed from the time history,as shown in Fig.17. Under external excitation, the maximum displacement of the cable structure is consistently significantly greater than that of the beam structure. The cable exhibits pronounced resonance at specific frequencies, with a significant increase in maximum displacement, while the beam's response is smaller and less sensitive. This aligns with the theoretical model discussed in Section 2. When the external excitation frequency is low (6 Hz to 8 Hz), the maximum displacement difference between the cable and beam structures under both sweep-up and sweep-down trends is not significant. Observing the time history curves of both shows that the natural frequency of the beam structure is relatively lower than that of the cable structure. At higher external excitation frequencies (13.5 Hz to 16.5 Hz), both the cable and beam structures exhibit more drastic changes in amplitude under sweep-up and sweep-down trends. Two significant jumps occur near 14.5 Hz, where the maximum displacement significantly decreases, indicating a significant dynamic amplification effect near this external excitation frequency.

6. Discussion and remarkable

6.1. The interaction between the cable and beam

Another intersting issue is the interaction between the cable and beam. In bridge engineering, finite element modeling of cable vibrations in cable-stayed bridges often involves these interactions. However, this interaction has not been elevated to the mechanical level, and its conceptualization remains unclear. Recently, Wang et al. [14, 20] derived the mechanical conditions from a variational perspective, providing the first mathematical description of cable-beam interaction and demonstrating the importance of mechanical conditions.

Therefore, it is particularly important to study the impact of cable-beam interactions. From the expressions of the coefficients of the nonlinear terms in the motion equations [14, 20], the quadratic nonlinear terms primarily arise from the initial configuration of the cable-stayed cables and the interactions between the cable and beam. For cable-stayed cables with relatively small sag, the quadratic nonlinear terms are mainly determined by the connection nonlinearity. Conversely, the cubic nonlinear terms in the system also involve interactions between the cable and beam but are less significant, mostly originating from the large geometric deformations of the cable-stayed cables and beams, with little relation to connection nonlinearity.

The study then proceeds without considering the interactions between the cable and beam for the structural 2:1 internal resonance response. By removing the interaction terms from the expressions of the quadratic and cubic nonlinear terms, the coefficients of the tuning equations are obtained for when local and mixed modes of the cable-beam occur in 2:1 internal resonance, considering and not considering interactions (see Tab.2). It is observed that the nonlinear coefficients considering interactions are mostly greater than those not considering interactions, reflecting the impact of structural interactions and leading to the quadratic nonlinearity of the cable-beam composite structure. This highlights the necessity of considering structural interactions.

Fig.18 shows the frequency-response curves of the first-order primary resonance of the cable-stayed beam, calculated using the nonlinear coefficients derived without considering interactions. Similarly, SN and HB denote saddle-node and HB points, respectively. Compared to Fig.3(a), which includes the effects of cable-beam interactions, it is clear that interactions significantly affect the system's dynamic performance, leading to notable changes in the resonance region. Without considering interactions, the system's response is relatively simple, characterized by fewer branches and more uniform amplitude changes, indicating a lower degree of structural nonlinearity. With interactions considered, the complexity of the system's response significantly increases, featuring more branching points and diverse amplitude trajectories. These results demonstrate that cable-beam interactions are crucial factors affecting the dynamic characteristics of cable-beam structures and thus should be fully considered in practical design and analysis.

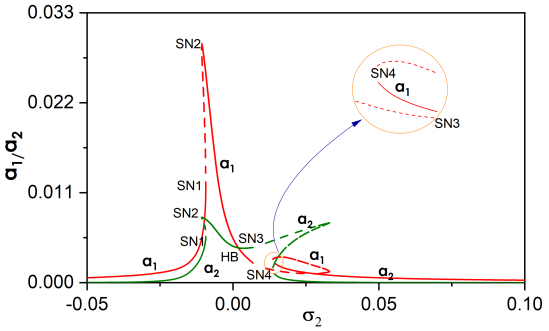

Figure 18: Frequency-response curve of the cable-stayed beam without interactions, $f_1 = 0.0001$, $\Omega \approx \omega_1$

Through the theoretical analysis in Section 2 and the above comparative analysis, the cable-beam interaction mainly involves the mechanical and geometrical conditions at the anchorage point, which have obvious effects on the self-oscillation characteristics and nonlinearities of the inclined beam. Theoretically, the stiffness of the cable and the beam differs significantly, making it impossible for their low-order natural modes to satisfy internal resonance in the traditional sense. However, the interaction influences the structural resonant characteristics, and there may be a clear proportional relationship between natural frequencies. As for the latter, mechanical conditions involve nonlinearities arising from the interaction. This nonlinearity has a certain impact on the nonlinear coefficients of the averaged equations and the system dynamics. Current discrete methods cannot account for this influence, emphasizing the importance of the method proposed in this paper. Additionally, this method can also be applied to nonlinear boundary conditions.

6.2. The effect of the beam nonlinearity

Assuming the interactions between the cable and the beam are ignored, this paper further explores the nonlinear effects of the beam structure. Based on the previously described expressions for nonlinear coefficients, the nonlinearity of the beam is observed to be caused by its large geometric deformations, which influence the coefficients of the cubic nonlinear terms, while the coefficients of the quadratic terms remain unaffected. By excluding the interaction between the cable and beam and the nonlinear components of the beam from the quadratic and cubic terms, we can obtain the coefficients of the tuning equations that consider the 2:1 internal resonance between local and mixed modes without including the effects of cable-beam interaction and nonlinearity, as shown in Tab.3. Unlike the results obtained by merely ignoring cable-beam interaction, the nonlinearity of the beam significantly impacts the S_{mm} term, suggesting that a detailed analysis of the beam's nonlinear coefficients and their specific effects on system response is necessary.

Fig.19 shows the frequency-response curves of the first-order primary resonance of the cable-stayed beam, calculated using the coefficients from Table 3 without considering the interactions between the cable and beam and the nonlinearity of the beam. Comparing Fig.3(a) (which considers both cable-beam interactions and beam nonlinearity) and Fig.18 (which only disregards cable-beam interactions), it is clear that the nonlinearity of the beam further significantly alters the dynamic characteristics of the system, particularly in terms of the soft and hard spring properties, leading to changes in the curve shape. The nature of the structural soft/hard spring properties depends on the dominant effect of the quadratic and cubic nonlinear terms during nonlinear vibrations; hence, an analysis is conducted focusing on the a_1 curve type. In Fig.3(a), with all characteristics of the structure preserved, the frequency-response curve shifts to the left across the entire response range, displaying soft spring characteristics, indicating that the effect of the quadratic terms is significantly greater than that of the cubic terms, and has a major impact on structural nonlinearity. When cable-beam interactions are removed, the degree of leftward shift in the frequency-response curve in Fig.18 is reduced, showing a trend towards linearity, i.e., a weakening of both soft spring characteristics and nonlinearity, indicating a diminished effect of the quadratic terms. This is consistent with the previous statement that "interaction terms mainly exist in the quadratic nonlinear terms." Therefore, the presence of cable-beam interactions enhances the structure's soft spring characteristics, further deepening the nonlinear response of the structure. Further removing the nonlinearity of the beam, the frequency-response curve in Fig.19 shifts to

Table 3
Coefficients of the tuning equations without the nonlinear effects of beams

Case	$K\times10^5$	ω_m:ω_n	Natural Frequency		Effective Nonlinear Coefficient					
			ω_m	ω_n	S_{mm}	S_{mn}	S_{nn}	S_{nm}	S_m	S_n
With nonlinear of beams	1.67	Global:Local	1.6743	3.3419	827.77	-4324.06	-36075.7	-59175.4	16.3	288
Without nonlinear of beams	1.67	Global:Local	1.6743	3.3419	-61.45	-1186.81	-35303.4	-15701	-10.97	-75.2

the right, displaying hard spring characteristics, causing the response curve to rise steeply. Summarizing the above analysis, cable-beam interactions and beam nonlinearity play significant roles in the system's dynamic response, leading to a shift in the dominance between quadratic and cubic terms, thereby changing the structure's soft/hard spring properties. This emphasizes the importance of thoroughly considering these factors when designing and analyzing cable-beam structures.

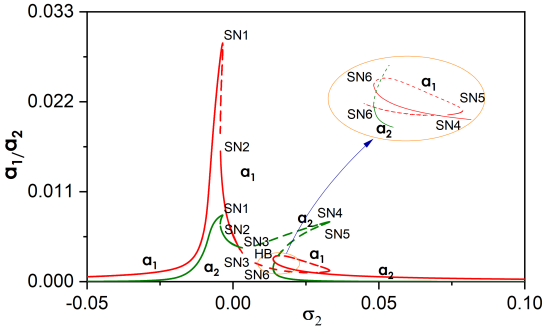

Figure 19: Frequency-response curve of the cable-stayed beam without the nonlinear effects of beam, $f_1 = 0.0001$, $\Omega \approx \omega_1$

6.3. Other internal resonance cases

It is worth noting that in Sections 4, there is a difference between the mixed-mode: localised mode and the localised-mode:mixed mode, although both are 2:1 internal resonances. Comparison shows that excitation acting on mixed modes often excites large amplitudes in local modes, whereas the same magnitude of excitation on local modes does not excite mixed modes as much. The fundamental reason is that the beam's stiffness is greater than the cable's, making it less prone to excitation. Notably, for forces acting directly on mixed modes, although the response of mixed modes is small due to the higher stiffness of the beam, the vibration of the beam at the connection causes two effects on the cable: axial elongation and lateral swinging. In fact, lateral swinging has a minor impact on vibration transmission, but axial elongation changes the cable force, which is the main reason for exciting the response of local modes.

Additionally, it should be highlighted that a 2:1 internal resonance can also occur between mixed and local modes. When the stiffness ratio is high, the beam's bending stiffness is greater, increasing the frequency of modes dominated or influenced by the beam's lateral vibration, while the order of the cable's local modes relatively decreases. Generally, the local modes of the cable are approximately integer multiples of each other. If the beam-dominated mode and the cable's local mode frequencies are in a 2:1 internal resonance, a crossing or veering phenomenon with another adjacent local mode will occur, evolving into a mixed mode. At this point, a 2:2:1 internal resonance involving three modes (mixed mode: local mode: local mode, or mixed mode: mixed mode: local mode) occurs. However, to understand the vibration mechanism, this discussion temporarily disregards any concurrent 1:1 internal resonance, focusing only on the 2:1 internal resonance between mixed and local modes.

7. Conclusion

This article investigates the multi-modal nonlinear response of cable-stayed beams with 2:1 internal resonance based on theory and experiments. Initially, the in-plane motion equations are derived using the variational principle. The nonlinear response is then solved using the method of multiple scales, and the nonlinear dynamics of the cable-stayed beam are analyzed with numerical results. The steady-state response and its stability of the cable-stayed beam are studied through frequency-response curves and force-response curves . The theoretical research results are further validated through experiments. The effects of the cable's static configuration and cable-beam interaction are also discussed. The research conclusions are as follows:

1. When the first-order mode is at primary resonance, the nonlinear response of the cable-stayed beam includes only two stable solutions. In contrast, during the second-order mode primary resonance, there exists a single-mode solution which loses stability through a pitchfork bifurcation, simultaneously giving rise to a bi-modal solution. At this time, the kinetic energy of the cable is transferred to the cantilever beam via 2:1 internal resonance, thus exciting the vibration of the beam, as confirmed by experimental results;
2. The equilibrium solution loses stability through a Hopf bifurcation and exhibits complex nonlinear dynamics. Periodic solutions may lead to chaos through a series of period-doubling bifurcations or change their stability through folding bifurcations;
3. In the modeling process of the cable-beam structure, whether using the classical theory's catenary line or the third-order approximation of the cable's static configuration, there is no significant difference in the resonance dynamics of the cable-stayed beam;
4. The interactions between cables and beams primarily involve the mechanical and geometric conditions at the anchorage points and are reflected in both the quadratic and cubic nonlinear terms, but mainly affect the quadratic terms. Ignoring cable-beam interactions leads to a reduction in soft spring characteristics and structural nonlinearity;
5. The nonlinear effects of the beam involve large geometric deformations, which are only reflected in the cubic nonlinear terms. Ignoring cable-beam interactions and further disregarding the beam's large geometric deformations lead to an increased dominance of the cubic terms, causing the structure's soft spring characteristics to transition to hard spring characteristics.

Finally, it is worth noting that in bridge engineering, the theory that parametric excitation leads to mathematical instability suggests it as a mechanism for large-amplitude vibrations in cables. This mechanism overlooks the overall vibrational response of the structure resulting from cable-beam interactions. Therefore, studying the 2:1 internal resonance of cable-stayed beams may provide a more comprehensive understanding of the mechanisms behind large-amplitude vibrations in cables.

Acknowledgements

The study was supported by National Natural Science Foudation of China (Grant No.12432001) and Provincial Natural Science Foundation of Hunan (Grant Nos. 2023JJ60527, 2023JJ30152) and the Natural Science Foundation of Changsha (Grant No. KQ2202133). The work of Prof. Lenci has been partially done within his belonging to the "Gruppo Nazionale per la Fisica Matematica", and within the "DICEA-Dipartimento di Eccellenza" project funded by Italian MUR.

References

[1] N. J. Gimsing, C. T. Georgakis, Cable supported bridges: Concept and design, John Wiley & Sons, 2011.
[2] H. Kang, Y. Han, J. Xu, Advances on dynamics and control in bridge engineering, J. Dyn. Control. 21 (2023) 1–6. (in Chinese).
[3] L. Zhang, G. Qiu, Z. Chen, Structural health monitoring methods of cables in cable-stayed bridge: A review, Measurement. 168 (2021) 108343.
[4] Z. He, W. Li, H. Salehi, H. Zhang, H. Zhou, P. Jiao, Integrated structural health monitoring in bridge engineering, Autom. Constr. 136 (2022) 104168.
[5] A. M. Martins, L. M. Simões, J. H. Negrão, Optimization of cable-stayed bridges: A literature survey, Adv. Eng. Software. 149 (2020) 102829.
[6] A. Javanmardi, K. Ghaedi, F. Huang, M. U. Hanif, A. Tabrizikahou, Application of structural control systems for the cables of cable-stayed bridges: state-of-the-art and state-of-the-practice, Archives of Computational Methods in Engineering 29 (2022) 1611–1641.

[7] Y. Wang, H. Kang, Y. Cong, T. Guo, T. Fu, Vibration suppression of a cable-stayed beam by a nonlinear energy sink, Nonlinear Dyn. 111 (2023) 14829–14849.
[8] Y. Wang, H. Kang, Y. Cong, T. Guo, T. Fu, Nonlinear dynamic analysis of a cable-stayed beam with a nonlinear energy sink, Acta. Mech. 235 (2024) 1921–1944.
[9] X. Wu, Y. Zhao, Z. Guo, L. Chen, Influences of temperature changes on global dynamical characteristics of suspended cables, J. Dyn. Control. 21 (2023) 32–40. (in Chinese).
[10] P. Warnitchai, Y. Fujino, T. Susumpow, A non-linear dynamic model for cables and its application to a cable-structure system, J. Sound Vib. 187 (1995) 695–712.
[11] V. Gattulli, M. Morandini, A. Paolone, A parametric analytical model for non-linear dynamics in cable-stayed beam, Earthq. Eng. Struct. D. 31 (2002) 1281–1300.
[12] Y. Cong, H. Kang, G. Yan, T. Guo, Modeling, dynamics, and parametric studies of a multi-cable-stayed beam model, Acta. Mech. 231 (2020) 4947–4970.
[13] X. Su, H. Kang, T. Guo, Y. Cong, Dynamic analysis of the in-plane free vibration of a multi-cable-stayed beam with transfer matrix method, Arch. Appl. Mech. 89 (2019) 2431–2448.
[14] L. Wang, X. Zhang, K. He, J. Peng, Revisited dynamic modeling and eigenvalue analysis of the cable-stayed beam, Acta. Mech. Sin. 36 (2020) 950–963.
[15] H. Kang, S. Meng, Y. Cong, T. Guo, X. Su, Investigation on dynamic modelling and nonlinear vibration behaviors of composite structures: A case of cable-beam model, Int. J. Nonlin. Mech. 166 (2024) 104871.
[16] T. Guo, G. Rega, Modal dynamics of boundary-interior coupled structures. part 1: A general approach using components green's function, Mech. Syst. Sig. Process. 149 (2021) 107230.
[17] T. Guo, G. Rega, Modal dynamics of boundary-interior coupled structures. part 2: An asymptotic interpretation of mode localization, Mech. Syst. Sig. Process. 149 (2021) 107248.
[18] Y. Fujino, P. Warnitchai, B. Pacheco, An experimental and analytical study of autoparametric resonance in a 3dof model of cable-stayed-beam, Nonlinear Dyn. 4 (1993) 111–138.
[19] Y. Xia, Y. Fujino, Auto-parametric vibration of a cable-stayed-beam structure under random excitation, J. Eng. Mech. 132 (2006) 279–286.
[20] L. Wang, J. Peng, X. Zhang, W. Qiao, K. He, Nonlinear resonant response of the cable-stayed beam with one-to-one internal resonance in veering and crossover regions, Nonlinear Dyn. 103 (2021) 115–135.
[21] V. Gattulli, M. Lepidi, J. H. Macdonald, C. A. Taylor, One-to-two global-local interaction in a cable-stayed beam observed through analytical, finite element and experimental models, Int. J. Nonlin. Mech. 40 (2005) 571–588.
[22] V. Gattulli, M. Lepidi, Nonlinear interactions in the planar dynamics of cable-stayed beam, Int. J. Solids Struct. 40 (2003) 4729–4748.
[23] M. Wei, Y. Xiao, H. Liu, Bifurcation and chaos of a cable–beam coupled system under simultaneous internal and external resonances, Nonlinear Dyn. 67 (2012) 1969–1984.
[24] Y. Cong, H. Kang, T. Guo, X. Su, Energy transfer between components of a cable stayed beam model under the concentrated excitation: 1: 2 modal resonance, Acta. Mech. Sin. 38 (2022) 521579.
[25] W. Lacarbonara, G. Rega, A. Nayfeh, Resonant non-linear normal modes. Part I: analytical treatment for structural one-dimensional systems, Int. J. Nonlin. Mech. 38 (2003) 851–872.
[26] A. H. Nayfeh, Nonlinear Interactions: Analytical, Computational, and Experimental Methods, Wiley Series in Nonlinear Science, Wiley, New York, 2000.